Temperature Inversion and Particulate Matter Concentration(PM10 Et PM2.5) in the Low Troposphere of Cergy-Pontoise (Parisian Region)

Souad Lagmiri * and Salem Dahech

Posted Date: 6 February 2024

doi: 10.20944/preprints202402.0319.v1

Keywords: Atmospheric Thermal Inversion; Radiosonde; Ground measurement; Pollution; PM2.5; PM10

Article

Temperature Inversion and Particulate Matter Concentration (PM10 et PM2.5) in the Low Troposphere of Cergy-Pontoise (Parisian Region)

Souad Lagmiti * and Salem Dahech

Research Center for the Organization and Dissemination of Geographic Information (PRODIG), UMR 8586 (CNRS), Paris Cité University, 75013 Paris, France.

* Correspondence: Souad.lagmiri@gmail.com

Abstract: This study aims to elucidate the influence of meteorological conditions on particle levels in Cergy-Pontoise. It explores the temporal variability of PM10 pollution days by associating them with the vertical temperature profile derived from conventional radiosondes from 2013 to 2022 (regional station). The results indicate that nearly 80% of exceedance days were associated with thermal inversions, primarily observed in winter and typically lasting 1 to 3 days. Analysis of winter thermal inversion characteristics suggests that those linked to pollution primarily occur near the ground, with higher intensity in December (12.1 °C) and lower in February (10.3 °C). Persistent inversions (extended nocturnal by diurnal inversion) account for 91.4% of the total inversions associated with high concentrations. Captive balloon soundings and temperature measurements at different altitudes were conducted during the winter of 2022/2023 to clarify thermal inversion in the Oise Valley at the center of Cergy-Pontoise. The results highlight three nocturnal wind circulation mechanisms in the valley, including downslope flow, circulation influenced by an urban heat island, and mechanical air evacuation under an inversion layer towards the less steep East side of the valley. Analysis of PM with the temperature gradient in the Oise Valley shows a significant correlation, suggesting an increase in concentrations during locally detected inversions and a decrease during atmospheric disturbance.

Keywords: atmospheric thermal inversion; radiosonde; ground measurement; pollution; PM2.5; PM10

1. Introduction

The temperature stratification in the lower troposphere influences the concentrations of gaseous and particulate pollutants [1]. When temperatures are higher at the surface than at altitude, meaning the gradient is adiabatic or super-adiabatic, atmospheric pollutants are dispersed towards higher layers [2]. However, a temperature inversion near the surface (first tens of meters of the troposphere) can form during specific situations [3–6]. Meteorologically, it is defined as a layer of air where temperature increases with altitude. The lower inversion level has significant consequences for the urban boundary layer and its chemical composition. If it is sufficiently distant from the ground surface, the inversion poses no risk of pollution over-concentration. On the contrary, a surface-level thermal inversion restricts the upward movement of air, promoting the accumulation of pollutants near the ground [7–10]. This can extend the duration and intensity of pollution, increasing risks to public health and the environment. The severity of this circumstance is particularly noted in the early winter mornings when emissions from heating and road traffic peak. In addition to surface inversions, descending air movements in the middle and lower troposphere compress the atmospheric boundary layer. The existence of these movements contributes to accumulating pollutants in an extremely thin layer. Given that the atmospheric layer has a positive lapse rate ($\Delta T/\Delta Z > 0$; where T represents temperature and Z represents altitude), turbulence is very

 doi:10.20944/preprints202402.0319.v1

low. Consequently, pollution is primarily of local origin, rather than a result of long-distance transport. Atmospheric stability conditions not only trap existing pollutants but also favor condensation and molecular nucleation processes. New secondary molecules appear during these situations of low dilution, especially in urbanized areas. Understanding the meteorological conditions responsible for triggering inversions is one of the primary keys to mastering the prevention of air quality deterioration and anticipating emission reduction measures.

The "radiation" type inversion often forms when longwave emissions from the surface lead to the cooling of the underlying atmosphere, while at altitude, the temperature increases. It occurs during nights with low wind speeds and clear skies. It dissipates shortly after sunrise. In some cases, especially during the winter solstice with limited sun exposure, the breakup of the inversion can be more challenging, resulting in the persistence of positive lapse rates during the day. Air temperature inversions are also associated with different types of synoptic circulation. There is the advection or frontal inversion, which forms under the influence of the downward movement of warm air masses and fronts [11,12]. The warmer air flowing over the cold air layer near the ground creates a positive temperature gradient that can sometimes reach 5 to 10 °C per 100 meters [13]. There is also the subsidence inversion, which forms when an air mass descends into the lower troposphere in an anticyclonic situation. During this subsidence movement, the temperature decreases less rapidly, and the air dries through adiabatic compression, resulting in a temperature inversion accompanied by reduced relative humidity [7]. This type of inversion can form at any time of the day around 1,000 to 2,000 meters high. When subsidence coincides with strong surface radiation, a composite inversion phenomenon can occur. This is characterized by a positive thermal gradient immediately from the surface to high altitudes. Inversion periods are characterized by the absence of wind and little or no sunlight. Often, the formation of fog and frost is observed, mainly due to airflow over wet areas leading to water vapor absorption. In topographically complex environments, such as valleys and mountains, inversions manifest as a layer of cold air [14–19].

The strength and persistence of inversions have been the subject of extensive research. Pernigotti et al. (2007) [20] found that the causes of persistent temperature inversions are often anticyclonic conditions, where a stable meteorological system keeps warm air stationary in the lower atmosphere over several days. Several researchers have emphasized that cities surrounded by mountains are particularly prone to persistent and pronounced temperature inversions [21–23]. These terrains have topography favorable to the accumulation of cold air due to both descending nocturnal thermal winds and ground cooling through longwave radiation [24,25]. Airflow is then blocked by natural obstacles for an extended period, making the air more stagnant. This explains the sustained extension of pollution episodes in complex urbanized terrains throughout the temperature inversion period [26].

The most frequently used techniques for measuring atmospheric profiles are satellite remote sensing, radiosondes, and observations from aircraft and drones [27–29]. Although satellite remote sensing offers broader spatial coverage, its coarse horizontal resolution limits its use in confined spaces. Radiosondes and aerial observations provide precise real-time information, but their spatiotemporal coverage is less extensive. Some studies also use meteorological stations at different altitudes to study the vertical structure of air temperature in a valley [30,31].

It is evident, based on the tools discussed above, that numerous previous studies have analyzed the mechanism of inversion formation in the troposphere at various altitudes. Several measurement campaigns dedicated to studying inversion properties in rugged terrains have been conducted, with a progressive focus on smaller scales [32,33]. However, our understanding remains limited regarding the accumulation of cold air in regions with less pronounced topography, such as gently sloping valleys with an altitude below 200 meters. Furthermore, the urban boundary layer in irregular terrains exhibits specific characteristics compared to a more flat topography urban zone. Even a slightly pronounced topography can create localized thermal winds, such as valley and slope breezes, which can influence the shape and size of the urban boundary layer. In plains, the urban layer is often more uniform in its height and composition. Therefore, measurement campaigns or experiments conducted in flat or rugged areas do not fully capture the dynamics of the atmospheric

 doi:10.20944/preprints202402.0319.v1

layer in a valley with less pronounced topography, such as our study area located in Île-de-France: the Cergy-Pontoise metropolitan area. In Île-de-France, there is only one radiosonde station (30km from our study area), and no studies have been conducted to explore the relationship between temperature inversion and air pollution in the Cergy-Pontoise metropolitan area.

The primary objective of the study is, therefore, to analyze how topographic features influence the dynamics of temperature inversion, focusing on air temperature variations in the lower troposphere at an altitude below 200 meters. Temperature variations and atmospheric stability, the subjects of this study, are two crucial factors for understanding particulate pollution concentration (PM10 and PM2.5). Consequently, this study provides an opportunity to examine the relationship between different types of inversions and pollution. The second objective of this study is to identify conditions under which PM10 and PM2.5 particle pollution persist for an extended duration. To achieve these goals, in addition to radiosondes, thermal and pollution measurements were conducted and analyzed over 2 months in the urban canopy, using temperature sensors installed on lighting poles.

2. Study area

This study focuses on the Cergy-Pontoise metropolitan area, located in Île-de-France in the greater Parisian suburbs at 49°02′20″ N and 2°04′37″ E. It constitutes a significant urban center in the Parisian region and is situated along the loop of the Oise River. The general terrain is characterized by the presence of valleys and extensive plains. Some isolated hills are noteworthy, especially to the north of the metropolitan area. The Oise River crosses the territory for approximately 18 km, passing through the heart of Cergy and irrigating the Ile de Loisirs, which spans 250 hectares (Figure 1.a). This location represents the lowest zone of the metropolitan area, with an altitude of about 19 meters. The hillsides of the Oise Valley exhibit pronounced slope changes to the west, with noticeable elevation differences of 50 to 70 meters. They are less steep to the east. The extreme north of the territory is affected by the Viosne Valley, which flows into the Oise at Pontoise. Almost all runoff waters from the territory flow towards the Oise via stormwater outlets. The Oise plain extends to the east of the territory, with an altitude not exceeding 50m. To the west, the Hautil massif represents the highest point in the region, reaching nearly 200 meters and offering a panoramic view of the area. Analysis of the topographic profile reveals a slope from north to south, ensuring optimal sun exposure across the entire territory. By analyzing the slope orientation map, it is determined that Cergy-Pontoise is a heterogeneous space characterized by different orientations (Figure 1.b). This geographical configuration, with its diverse slope orientations, has an impact on sunlight exposure and creates thermal variations that can have significant consequences on the local climate and pollutant accumulation.

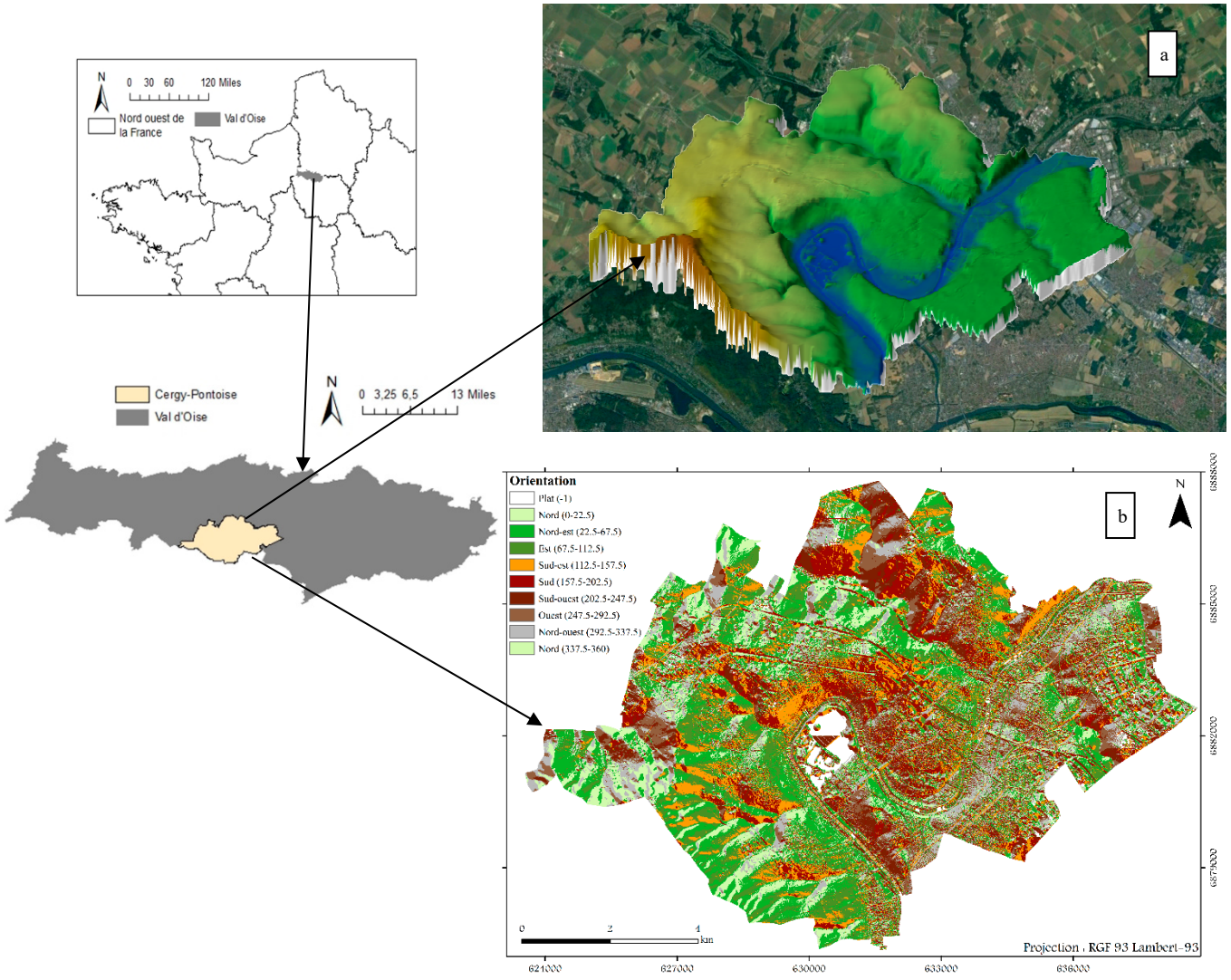

Figure 1. Geographic location of the Cergy-Pontoise urban area. (a) Topographic map; (b) Slope orientations map.

doi:10.20944/preprints202402.0319.v1

 doi:10.20944/preprints202402.0319.v1

From an urban planning perspective, the topography marked by the Oise Valley has influenced the building expansion pattern in the metropolitan area. Over a total area of 84.20 km2, urbanization has encroached on 57% of the territory (INSEE 2012 data), primarily along gentle slopes conducive to soft mobility (especially cycling). The most densely populated urban areas are situated on a fairly regular slope from east to west. These areas mainly feature collective buildings of the "cités" and "small unit residences" types. The steep hillside zone has a low urbanization density and fairly dense vegetation cover. Developments close to the Oise riverbank have seen limited expansion due to the risk of flooding. Additionally, to the west of the metropolitan area, the Hautil Forest plays a significant role, adding a substantial natural space to the urban agglomeration.

Cergy-Pontoise benefits from a moderated oceanic climate, with the moderating influence of the ocean resulting in cool to mild winters and temperate summers. Temperatures are relatively mild, with average differences of around 15 °C between summer and winter, and an annual temperature of approximately 11 °C. Precipitation is consistent throughout the year, occurring on average for 115 days annually, with an average annual accumulation of 650 mm. Sunshine is significant for much of the year, with approximately 1729 hours of sunshine per year, including 700 hours during the warm season. Situations characterized by clear skies and weak winds, favorable for the establishment of a temperature inversion, are unevenly distributed throughout the year. Over 30 years (from 1991 to 2021), there is an observed occurrence of around 20% of calm situations conducive to inversions, with more frequent situations between August and October.2. Materials and Methods

In the urban area, there is no regular measurement of the vertical temperature profile. The only available readings come from the Trappes station, located 30 km from the study area. Since Trappes and Cergy-Pontoise have similar topographical characteristics, the soundings conducted in Trappes are also representative of Cergy-Pontoise, especially during anticyclonic meteorological situations that can be generalized to the entire region. The data is downloaded from the Meteociel weather data platform (https://www.meteociel.fr/observationsmeteo/sondage.php?archive=1&map=0&jour=23&mois=9&annee=2014&heure=0&mode=&sub=OK). In this study, Trappes soundings are used to reconstruct the history of temperature inversions from 2013 to 2022, responsible for triggering PM10 pollution episodes (PM2.5 data is not available) recorded by the AirParif station (a conventional pollution measurement station installed in the heart of Cergy).

To provide information at the local scale, five "Ecosmart" type sensors for climatic parameters (Temperature, Humidity, Pressure) and certain pollutants such as PM are installed in Cergy-Pontoise. The measurements provided by these stations help identify areas where cold air accumulates in the valley and deduce the presence of temperature inversions. For this purpose, ground temperature data for the winter of 2022/2023 (December and January) are collected from the five sensors placed on a slope ranging from the center of the basin to the east and west sides (Figure 2). The slope on the west side of the basin is steeper than that on the east side. Its altitude varies from 19 to 154 meters, while that of the east slope varies from 19 to 42 meters. It is relevant to mention that the sensors are installed at a height of 3 meters above the ground on lighting poles. The data is continuously transmitted via a cellular network. However, the sensor shelters are not certified and do not have sufficient ventilation, making the recordings unreliable during the day. Therefore, only nocturnal climatic parameters are considered in this study. The temperatures recorded during the night at different altitudes are used to calculate the temperature difference (ΔT) between the high-altitude station (A) and the low-altitude stations (B, C, and D). Then, the ratio of the temperature difference to the altitude difference ($\Delta T/ \Delta Z$) is calculated. This ratio called the "decay rate," is then compared to the adiabatic decay rate ($\gamma adiab$ = -0.01 °C°m^{-1}) and the isothermal value ($\gamma isotherm$=0 C°m^{-1}) to examine the air mass along the two peripheral slopes of the basin (equation 1 and 2). These stations have similar environmental characteristics in terms of land use, being mostly sparsely urbanized, except for zone D, which is more heavily urbanized. In this experiment focused on the impact of altitude and relief shape on temperature, the heat flux generated at the D station level is also taken into account to explain the temperature variation.

Preprints.org (www.preprints.org) | NOT PEER-REVIEWED | Posted: 6 February 2024 doi:10.20944/preprints202402.0319.v1

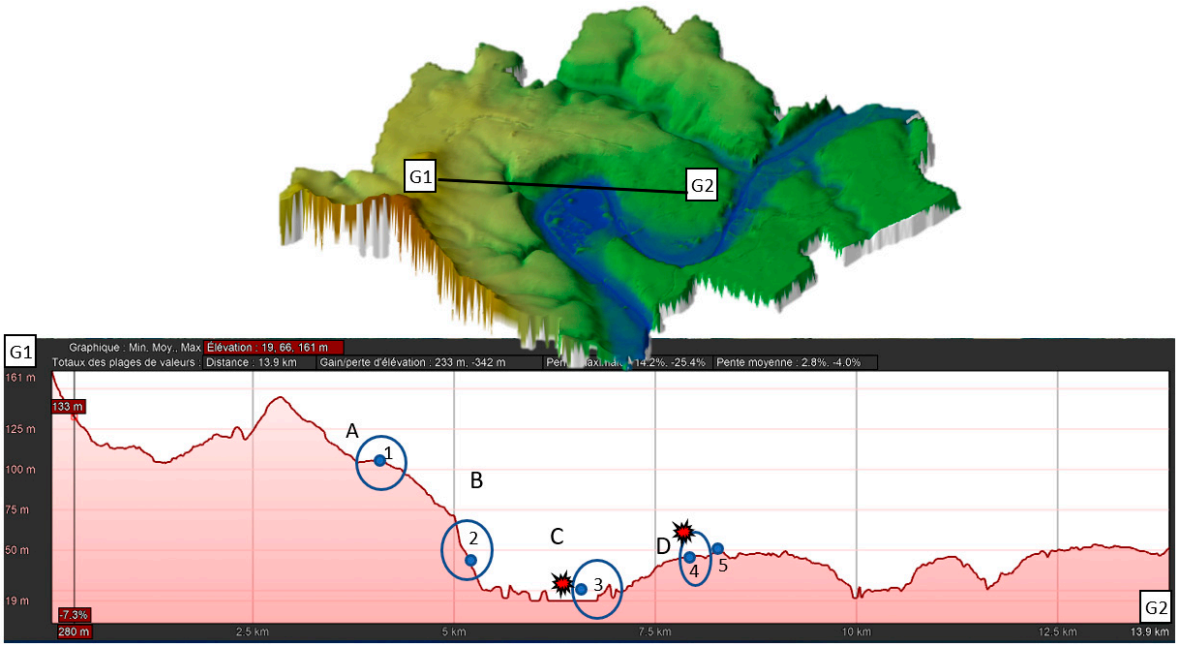

Figure 2. Topographic profile of the study area and locations (A, B, C, and D) of climate and pollution parameter measurement stations (numbers indicate each sensor's identifier). Red stars represent Davis stations.

To determine the spatial extent of temperature inversions, data from Trappes were compared with ground-level measurements taken by Ecosmart sensors. Inversions, co-occurring at both locations were identified as regional inversions, covering the entire urban area, while those occurring at only one of these locations were considered local.

$$\Delta T_i = T_A - T_{i\,(i=B,C,D)} \quad \Delta Z_i = Z_A - Z_{i\,(i=B,C,D)} \quad (1)$$

$$\Delta T/\Delta Z \leq \gamma_{adiab}\ \text{(Unstable air mass)}, \quad \Delta T/\Delta Z > \gamma_{isotherme}\ \text{(Temperature inversion,} \quad (2)$$

To design the vertical profile of the free air in the basin's center, a series of radiosonde observations were conducted using captive balloons from the basin floor to altitudes of approximately 147m above sea level. Descending soundings were performed every 10 minutes at altitudes of 147m, 110m, 67m, 52m, and 42m, using a thermal sensor attached to the balloon. These heights were calculated using the following equation:

$$h = tg\,a \times c. \quad (3)$$

"(h) balloon height, (c) length of the side opposite the angle (a). Since the calculation of the balloon height (h) was based on a visual estimation of the length of the side (c) opposite the angle (a), we accept an average margin of error of 2 meters."

In parallel with the radiosondes, we conducted continuous measurements of temperature and humidity using ground-level sensors and sensors positioned at a height of 2 meters. Additional meteorological measurements were carried out to address questions related to thermal stratification, utilizing two 'Davis' type weather stations. The first station is located at the bottom of the 'Idl' basin in a vegetated area at an altitude of 3 meters, while the second is positioned in an urban location at an altitude of 42 meters from the bottom of the valley on the roof of a building called 'mgen' on the east side of the basin. These stations record average temperature, relative humidity, dew point, wind direction, and wind speed every hour.

To study the correlation with pollution, we analyzed data from Ecosmart sensors that measure concentrations of PM10 and PM2.5 every minute using the combined optical component. To eliminate point source pollution, we performed preprocessing by calculating the hourly median value. These sensors are calibrated using analyzers accredited by CLAQM (Central Laboratory for Air Quality Monitoring) and verified annually according to ISO 17025 standards.

3. Results

 doi:10.20944/preprints202402.0319.v1

3.1. Temporal Variation of Pollution and its Relationship with Thermal Inversion

From 2013 to 2022, the AIRPARIF station in Cergy recorded 87 days during which the daily limit value for PM10, set at 45 µg/m³, was exceeded (see Table 1). Approximately 80% of these exceedance days (70 days) were associated with thermal inversion situations and the years 2013 and 2016 had the highest number of exceedance days related to thermal inversion, with 17 and 11 days respectively. They were followed by the years 2014 and 2017, each recording 9 exceedance days. However, since 2020, the number of these days has been relatively low, ranging between 2 and 5 days per year. Except for the year 2018, all years with more than 8 thermal inversion days showed higher average concentrations, ranging from 59.1 to 65.8 µg/m³. In contrast, years with fewer than 5 thermal inversion days (from 2020 to 2022) exhibited lower concentrations, not exceeding 50.9 µg/m³. Thermal inversion events associated with exceedances mainly appear as short-duration inversions, lasting 1 to 3 days per episode, as illustrated in Table 1 and Figure 3. Only 5 episodes out of 35 were persistent, lasting 4 to 6 days. These episodes occurred in 2016, 2017, and 2019, with one episode per year. The two longest episodes, lasting 5 and 6 days, occurred in 2013 and 2014 respectively. Therefore, it is evident that pollution levels are not solely influenced by the number of inversion days at the regional scale, but also seem to vary based on other factors such as local atmospheric stability, as discussed in the Detection of Inversions in the Oise Valley section.

Table 1. Annual Variation of Pollution Days and Types of Episodes Linked to Thermal Inversion. The annual concentration is calculated based on exceedance days.

Year	PM10 (µg/m³)	Days of pollution without inversion	Days of pollution with inversion	Pollution episode with inversion	Type of episode
2013	**59.07**	5	**17**	**11**	s1,s2,s3,**s5**
2014	**65.81**	3	**9**	**3**	s1,s2, **s6**
2015	57.39	2	6	**3**	s2,s1,s3
2016	**62.89**	1	**11**	**5**	s1,s2,s3,**s4**
2017	**62.11**	1	**9**	**3**	s2,s3,**s4**
2018	51.71	2			
2019	51.95	1	**8**	**4**	s1,s2,**s4**
2020	50.88		2	**1**	s2
2021	49.69		5	**3**	s1,s2
2022	48.97	3	3	**2**	s1,s2
Total		18	70	35	

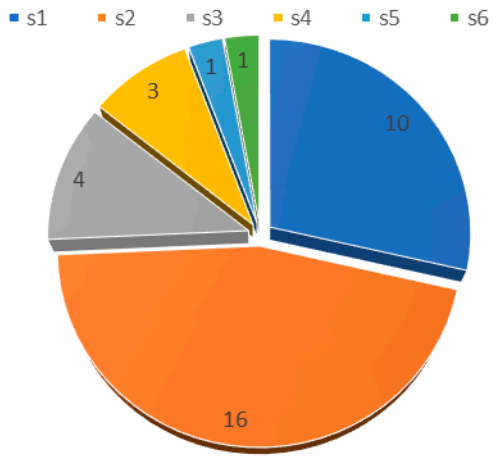

Figure 3. Pie chart summarizing the distribution of the number of episodes for each type.

The monthly variation in the number of pollution days reveals an absence of fine particulate matter (PM10) pollution during the summer season and the month of October. While radiative conditions conducive to high concentrations of primary pollutants are more frequent in summer, the

Preprints.org (www.preprints.org) | NOT PEER-REVIEWED | Posted: 6 February 2024 doi:10.20944/preprints202402.0319.v1

lack of exceedances is partly explained by the low volume of road traffic. Summer remains the time of the year with the least dense traffic on road networks. According to data collected over three consecutive years (from 2017 to 2019), the month of August saw a 21% reduction in the number of vehicles on national roads, while on the departmental network, this decrease reached 18%. A similar reduction of 16% is also observed on the highway network [34].

The absolute maximum concentrations are observed in December (68 µg/m³), January, and March (60 µg/m³). They hover around 50 µg/m³ for the rest of the year. From November to February, pollution episodes are triggered by thermal inversions, with 6, 18, 18, and 13 inversion days per month, respectively (Figure 4). In March, the increase in concentrations may be due, in addition to thermal inversion, to biological activity. On average, one day per month experiences a thermal inversion in April, May, and September. This number starts to increase from November and reaches its maximum in December/January with 18 days. This frequency of occurrence indicates a significant upward trend in the inversion phenomenon, especially during the cold season.

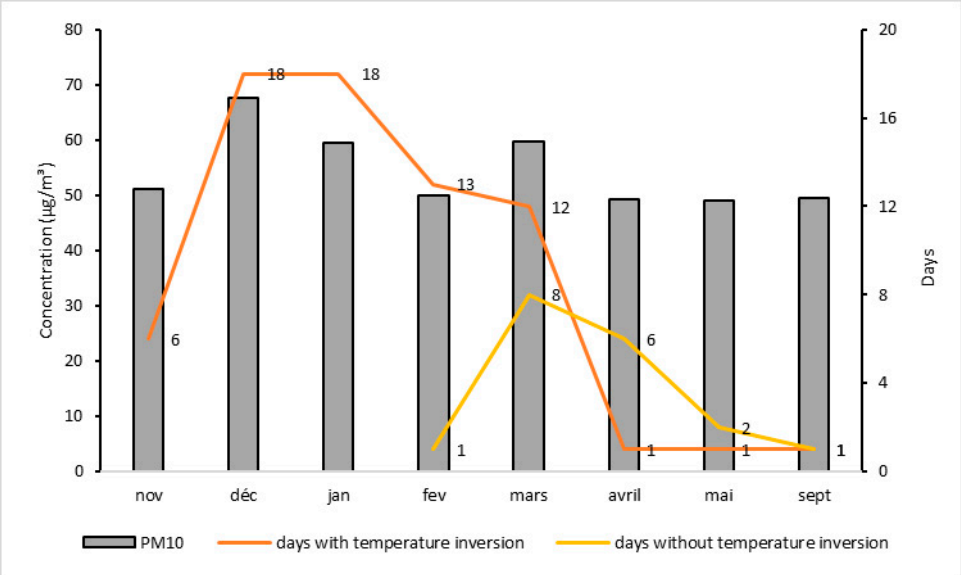

Figure 4. Monthly variation in average concentrations and pollution days (AIRPARIF data from 2013 to 2022).

3.2. Temporal Variation of Inversion Properties

In this section, we examine inversions related to exceeding the daily PM10 threshold recommended by the WHO, analyzing their depth, intensity, and base altitude. Our analysis is limited to December to March, during which the number of inversion days is highest. Figure 5 illustrates the statistical distribution of these variables during this period. During winter, the depth of inversions shows significant variability, with observations indicating deeper inversions in January and shallower ones in February, based on median and mean values. In January, the median and mean depth of inversion is approximately 380 meters. In February, the inversion depth ranges from 57 to 510 meters, which is the lowest range compared to other months. Its median value is about 139 meters, and its mean is about 196 meters. The inversion depth exhibits the greatest variability in December, ranging from 115 to 929 meters. This month has a median value quite close to that of March (about 293 meters) and a slightly higher mean (359 meters compared to 277 meters).

Preprints.org (www.preprints.org) | NOT PEER-REVIEWED | Posted: 6 February 2024 doi:10.20944/preprints202402.0319.v1

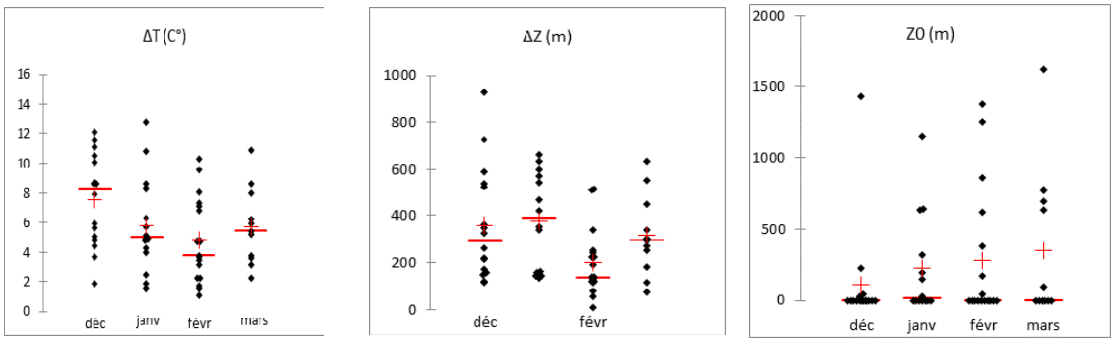

Figure 5. Scatterplots of inversion intensity (ΔT), depth (ΔZ), and base (Z0) during pollution days (Trappes radiosonde data, 2013-2022).

December has the least variability in inversion base heights. Most heights are at ground level. Two exceptions are noted: one inversion at 1434 meters and one at an altitude of 224 meters. Generally, the median value of the inversion base height is at ground level for all months. The average altitude of the inversion base gradually increases from 108 meters to 347 meters. About 58.6% (41 days) of inversion days have a base at ground level, and 15.7% (11 days) have a base between 25 and 318 meters. These results suggest that in Trappes, inversions responsible for pollution are generally close to the ground. Sometimes, inversion base heights are biased towards higher altitudes. Approximately 11.4% of inversion days (7 days) have heights between 382 and 774 meters. Subsidence or frontal origin inversions are observed for about 12.9% (9 days). The maximum inversion base height is observed in March at 1621 meters, followed by February at 1385 meters.

To explore the strength of these inversions, the intensity of inversions is assessed by measuring the temperature difference between the upper and lower layers of the inversion. Overall, there is relatively high variability in the intensity of inversions during the four months considered. The temperature medians are 8.25 °C in December, 5 °C in January, and 4.7 °C in February and March. Maximum values are observed in early winter with 12.1 °C in December and 12.8 °C in January. Towards the end of winter, the maximum intensity decreases to reach 10.3 °C in February and 10.9 °C in March. Inversions are more pronounced in December, with an average of 7.5 °C, and weaker in February (average of 5.2 °C).

3.3. Daily variations in thermal inversion

Thickness and intensity of inversions were measured for pollution days at midnight and noon each winter from 2012 to 2022 (The gap rate for noon data is 2.85%). Over the 10 winter seasons, significantly thicker inversions were recorded during the night compared to daytime inversions, with particularly high values during the winters of 2012/2013 (418m), 2015/2016, and 2021/2022 (390m) (Figure 6a). The thickness of inversions varied at both measurement times. Overall, nighttime thickness ranged from 243 to 418m, while daytime thickness ranged from 186 to 347m. The winters of 2018/2019 and 2019/2020 were characterized by less thick nighttime inversions, while daytime inversions were weaker starting from the winter of 2018/2019. The last two winter seasons, as well as the winters of 2012/2013 and 2015/2016, proved to be atypical as the inversion layer showed a significant thickness shift between night and day, ranging from 110 to 180m.

The average intensity of nighttime inversions ranged from 4 to 7.6 ◦C, and daytime inversions from 3 to 5.9◦C. The greatest variability between winters was observed for nighttime inversions, with a maximum of 7.6 °C during the winter of 2018/2019 (Figure 6b). The highest intensity of daytime inversion occurred during the winter of 2012/2013, reaching 5.9 °C, slightly higher than nighttime intensity (5.3 °C). However, during other winter seasons, nighttime inversions showed greater intensity. During the winter season of 2018/2019, the intense inversion layer recorded during the night is characterized by a relatively thin thickness. In contrast, inversions in the winters of 2013/2014 and 2014/2015 had thick layers but were less intense. This indicates that the previously mentioned thick inversions are not necessarily the most intense. However, the most intense nighttime inversions are recorded from the winter of 2018/2019 onwards.

 doi:10.20944/preprints202402.0319.v1

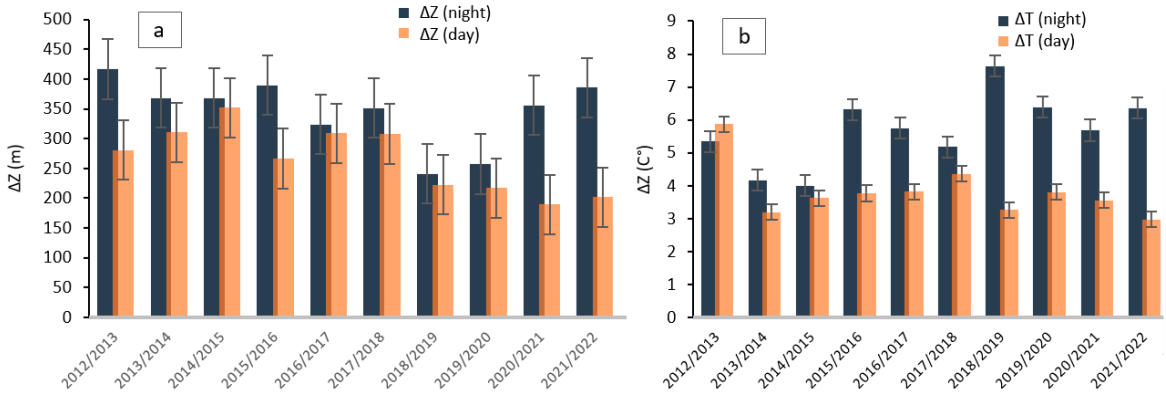

Figure 6. Depth (a) and intensity (b) of nighttime and daytime inversion layers during the cold season, from November to February over the period 2012-2022; the number of cases is 70 days.

3.4. Typical vertical profile of inversion

Based on 70 days of inversions (corresponding to pollution days) detected from 2012 to 2022 in Trappes by radiosondes, we studied the frequency of persistent inversions. The frequency of inversions that persist with the arrival of the day (extended nocturnal inversion followed by a diurnal inversion) represents 91.4% of the total inversions, while those solely nocturnal do not exceed 9.6%. This leads to the conclusion that days of PM10 pollution are mainly induced by prolonged inversions. It also suggests that when a persistent inversion occurs, a PM10 pollution episode will be systematically generated.

Figure 7 shows a case of inversion on January 21/22, 2017. It corresponds to a vertical profile of air temperature with typical nocturnal and diurnal inversions. During the night, the inversion reaches a depth of 541 m (from 168m to 709m) and an intensity of 8.8 °C. Thus, the vertical temperature gradient calculated over the entire inversion layer is +1.62°C/100 m. Throughout the inversion layer, the dew point temperature (relative humidity) decreases with altitude, ranging from -5.8 °C to -12.6 °C (from 84% to 27%) between the base and the top of the inversion. The wind blows from the southeast, and its speed is low. Near the surface, it does not exceed 1.8 km/h, and at the top of the inversion, it reaches 9.4 km/h. Turbulence becomes more significant in the layer above the inversion (from 709 to 2442m) with an average speed of 21.3 km/h and a direction oriented towards the south. This second layer is characterized by an increase in humidity with altitude and a thermal gradient (-0.75°C/100 m) approaching the dry adiabatic gradient (-0.98°C/100 m).

During the day, the inversion contracted in depth by 266 meters and in intensity by 3.2°C. At an altitude above 488 meters, the temperature gradually decreases by about -0.35°C/100 meters, and beyond 1068 meters, this rate approaches that observed at night, namely -0.69°C/100 meters. At ground level, the wind blows from the north at a speed of 9.4 km/h, while at altitude, it comes from the northeast with a more pronounced strength of 31.3 km/h. Similar to the nocturnal inversion layer, the dew point temperature and relative humidity decrease with altitude, ranging from -3.1°C to -18.7°C for the dew point and from 73% to 16% for relative humidity. Overall, the inversion layer is characterized by a less calm and less humid atmosphere during the day than at night. The unstable layer just above the inversion has a wind direction from the northeast and an average speed of 25.9 km/h.

Preprints.org (www.preprints.org) | NOT PEER-REVIEWED | Posted: 6 February 2024 doi:10.20944/preprints202402.0319.v1

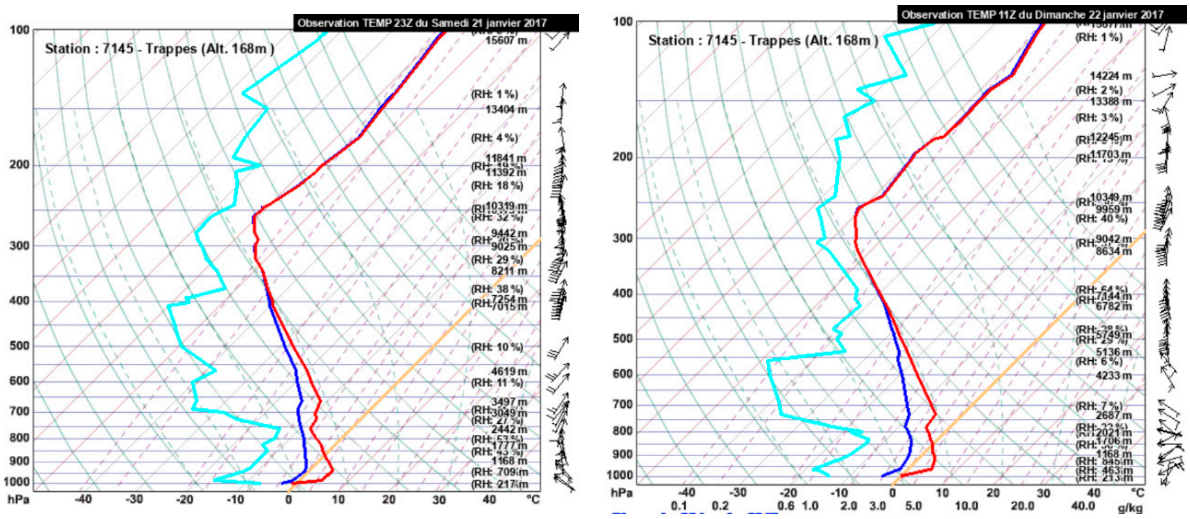

Figure 7. Vertical profile of air temperature, dew point, humidity, and wind during a typical situation of nocturnal and diurnal inversion. (Skew-T log-P diagrams from radiosondes conducted by Trappes on January 21/22, 2017).

3.5. Detection and Dynamics of Inversions at the Local Scale

In this section, the inversion intensity at the local scale is analyzed based on ground-level temperature observations at different altitudes in the Oise Valley. The chosen period for this study extends from December 2022 to January 2023. This method could provide information about areas of fresh air accumulation in the study area and indirectly indicate the presence or absence of inversions.

The results of the temporal variation in the $\Delta T/\Delta Z$ ratio for the three "Ecosmart" station combinations calculated relative to station A (AB, AC, and AD) show that several nights in December 2022 and January 2023 are consistently stable ($\Delta T/\Delta Z > \gamma_{adiab}$) (Figure 8). They often exhibit a temperature inversion between station A and stations B and C ($\Delta T/\Delta Z > \gamma_{isotherm}$). The stability and less frequent inversions at D are attributed, on one hand, to the nature of the substrate and, on the other hand, to the station locations on an inclined surface, promoting the drainage of fresh air into the basin area. The consistently high positive values of the $\Delta T/\Delta Z$ ratio observed for several consecutive days illustrate the presence of persistent inversions between the two altitude levels considered.

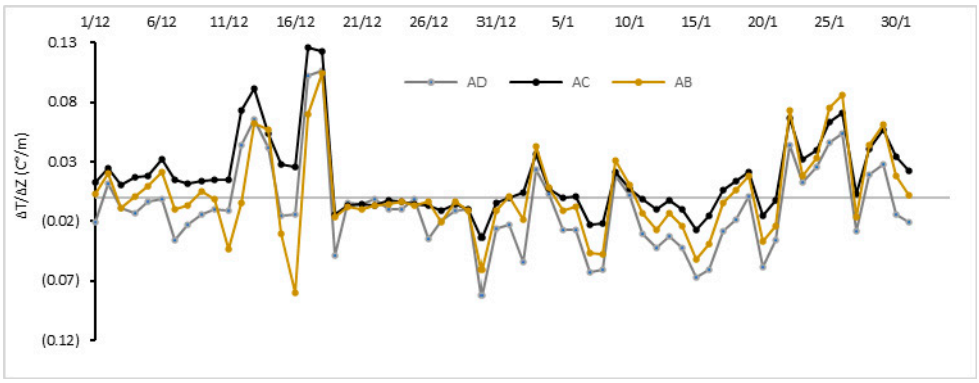

Figure 8. Temporal series of ($\Delta T/\Delta Z$) calculated at midnight from 01/12/2022 to 31/01/2023 (data from the 5 fixed stations).

3.6. Consistency between the inversion observed in Cergy and that in Trappes

The relatively strong correlation (between 0.83 and 0.96) among the three $\Delta T/\Delta Z$ ratios calculated concerning stations A, B, C, and D is fascinating (Table 2). It is thus possible to assess the

Preprints.org (www.preprints.org) | NOT PEER-REVIEWED | Posted: 6 February 2024 doi:10.20944/preprints202402.0319.v1

state of the atmospheric layer tangent to the ground along the slopes, taking the average of the three ratios:

Table 2. Correlation coefficients between the ΔT/ΔZ ratios for the three pairs of stations.

Ratios	AD	AC	AB
AD	1		
AC	**0.96**	1	
AB	**0.87**	**0.83**	1

$$\Delta T/\Delta Z_{global} = \frac{1}{3}\sum_{At}^{t=B,C,D}(\Delta T/\Delta Z)_{At} \quad (4)$$

Figure 9 depicts the temporal evolution of this average ($\Delta T/\Delta Z_{global}$). The ratio calculated from the Trappes station ($\Delta T/\Delta Z_{00h}$) is also projected in the figure. Note that only the ratio for nights with inversion is calculated. In total, 27 nights with inversion are considered, and evidently, 35 nights without inversion (5 nights without data) have been excluded. The winter average (γwinter = 0.017°Cm^{-1}) calculated from the data of 10 winter seasons (from 2012 to 2022) is also represented in the graph. The goal is not to seek correlation between the two types of data (Trappes and Ecosmart) but rather coherence between the two considered scales to assess the spatial extent of the inversion. The graph shows that periods with $\Delta T/\Delta Z_{global}$ values higher than the winter average (γwinter = 0.017°Cm^{-1}) are generally consistent with the occurrence of inversions captured by the Trappes station. This suggests that strong temperature gradients calculated on a slope can be considered a measure to infer the occurrence of an inversion covering the entire urban area (see example in photo No. 1. a). Inversions calculated from the Trappes station that do not coincide with positive values of $\Delta T/\Delta Z_{global}$ correspond to inversions distant from the surface. Gradients lower than γ_{winter} (0.017°Cm^{-1}) and higher than the isotherm value ($\gamma_{isotherm}$ = 0°Cm^{-1}) isolate nights with a shallow and non-persistent inversion at the ground level. They may correspond to advection inversions near the lowest part of the urban area where cool air masses accumulate under the warm air from the plateau (see example in photo No. 1. b). Dates with negative values (less than γ_{adiab} = -0.01°Cm^{-1}) indicate a disturbed atmosphere.

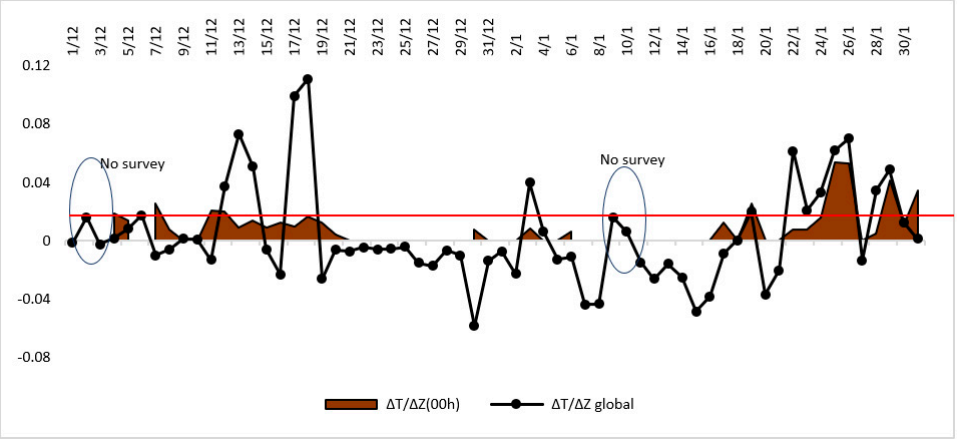

Figure 9. Time series of the ΔT/ΔZglobal ratio calculated from the 5 ground stations (in black) and the ratio calculated from the radiosondes of the Trappes station (in brown). The red line represents the winter average (γwinter = 0.017°C/m^{-1}).

 doi:10.20944/preprints202402.0319.v1

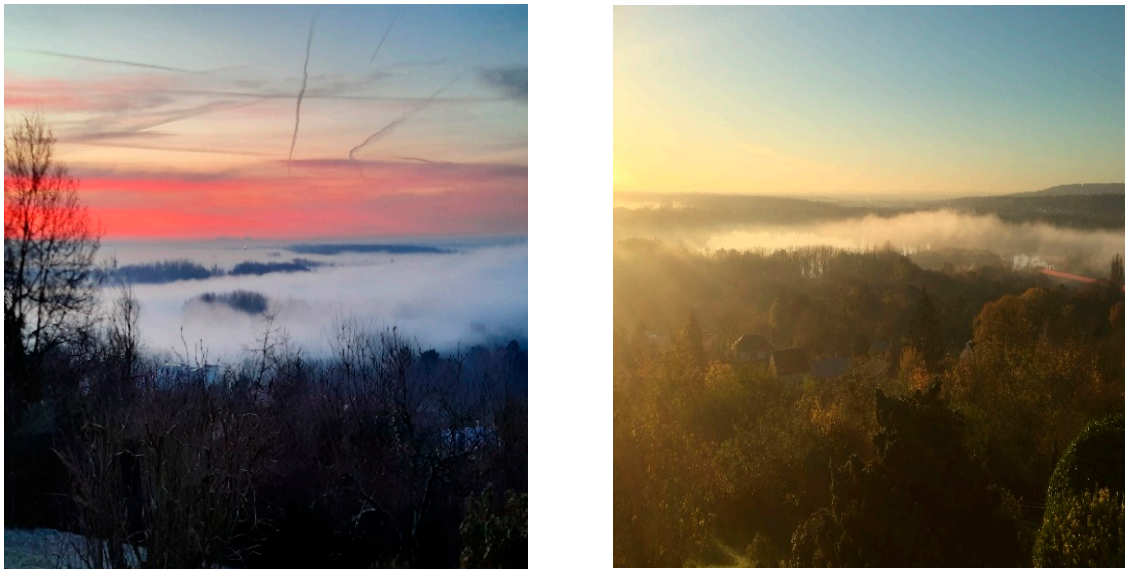

Photo n°1: picture (a) taken on February 13, 2022, showing the cold air lake covering the entire urban area; picture (b) taken on November 2, 2022, during a situation of cold air advection near the lowest part of the urban area.

3.7. Coherence between the inversion observed by the Ecosmart stations and the captive balloon-sounding

Figure 10 displays temperatures averaged every 10 minutes from 7:10 to 8:06. These measurements were conducted using a sounding balloon launched on March 2, 2023, in the leisure base, during an anticyclonic situation favorable to thermal inversion. It is noteworthy that these measurements are used to represent the inversion structure in the valley. The vertical distribution of air temperature at three altitudinal levels (110m, 2m, and 0.5cm) at 7:20 shows a strong thermal inversion (ΔT= 2.32+0.45). The thermal gradient reaches 2.77°C/110m with the base at ground level. Filling the information gap for intermediate levels between 2m and 110m began at 7:35. Results show that the temperature at ground level (0.5cm) and at 2m continuously decreased until 7:49. At 8:06, the thermal inversion between the ground and 25m altitude is maintained. It is worth mentioning that the valley is characterized by a gentle slope on the East side, reaching a maximum height of 25 meters, classifying it as semi-open with an air outlet oriented towards the East. Tracking the balloon trajectory and wind direction recorded by the Davis station on the roof of the "Mgen" building confirmed this air outlet. It can also be observed that from 7:41 to 8:06, the temperature increases with altitude; indeed, the temperature is lower in the upper levels than the lower levels between 45m and 25m. This is attributed to a weakening of the inversion above the maximum height of the East slope. This weakening is due to the evacuation of fresh air by horizontal flows with an intensity of about 1.3 m/s and a west-northwest direction. These flows result from the thermal contrast between the most rural area of the agglomeration to the north/west and the most urban area to the east, thus inducing a countryside breeze, confirmed by field observations. Note that the rural fringe is situated at a higher altitude compared to the urban fringe.

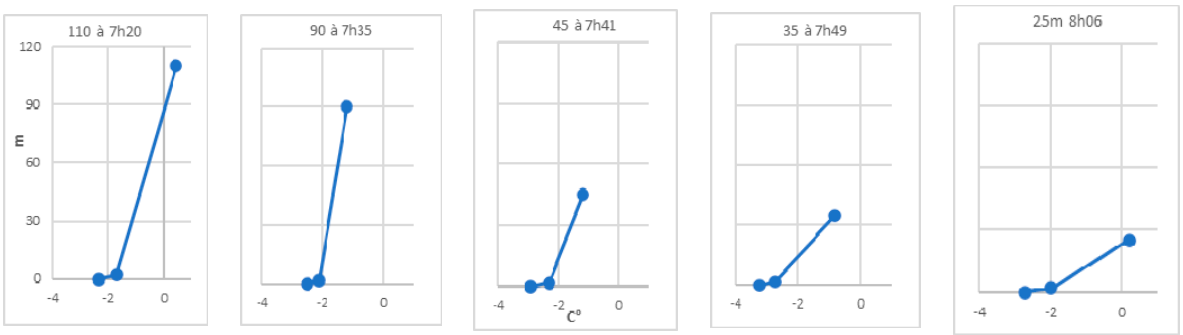

 doi:10.20944/preprints202402.0319.v1

Figure 10. Vertical distribution of air temperature taken at intervals from 7:20 to 8:06 (radiosonde balloon sounding on March 2, 2023).

The comparison of sounding temperatures (from 7:35 to 8:06 on March 2, 2023) with those of the slope line is illustrated in Figure 11. Since the inter-valley circulation induced by the slope flow cannot be considered two-dimensional, temperatures on the East and West slopes are considered separately. The results show that temperatures on both slopes below 25m are a good indicator for free air temperature soundings in the center of the basin, with a standard deviation of 0.35 for the East slope and 0.38 for the West slope. This area corresponds to the zone of cool air settling. The higher temperatures observed on the East slope are due to the urban heat island effect. The highest biases are mainly noted on the west slope at 90m where the air is relatively cooler. They could be related to the downward movements of cool air towards the ground. Figure 11 presents a simplified diagram of the cool air accumulation process and the flows generated in the studied basin.

Quantitative comparisons between temperature profiles in the center of the basin and along the two slopes below 25m reveal low errors recorded in terms of the intensity of the thermal inversion. Thus, measurements along the East and West slopes are suitable for detecting the formation of inversions in this area. Although it is evident that some accuracy is lost in the upper layers of the basin compared to the vertical profile obtained in the center of the basin, significant advantages are gained in terms of identifying microclimates through the use of surface-based temperature sensors.

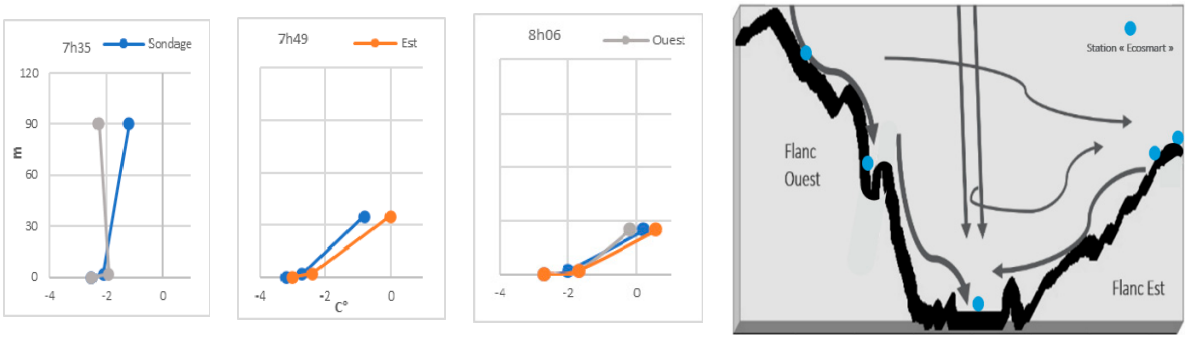

Figure 11. Temperature differences between free air and the air mass along the slopes of the Oise Valley. The diagram on the right illustrates the flows generated in the basin during stable weather.

3.8. Link with Particulate Pollution

For the period from December 2022 to January 2023, the thermal inversion occurs a little more than every other day (55%, or 34 out of 62 days). A percentage of 35% of the inversion days (22 nights) have a global ratio $\Delta T/\Delta Z$ higher than the winter average; thus, they are strongly stable with a high inversion intensity ($0.017 < \Delta T/\Delta Z < 0.12$). Among the 34 inversion days, 12 appear to be periods of transition or advection inversion of air masses between the upper and lower parts of the urban area.

We have overlaid on the same diagram the daily concentrations of PM10 and PM2.5 (measured from stations B, C, and D) to determine if locally detected inversions were significantly correlated with each pollutant (Figure 12). As seen, there is a slightly strong significant correlation (Pearson) with PM10 (0.59) and PM2.5 (0.60). Except for a few exceptions, high concentrations (above 80 µg/m³ for PM2.5 and 100 µg/m³ for PM10) occur during thermal inversion situations. Concentrations below the WHO standard (45 µg/m³ for PM10 and 15 µg/m³ for PM2.5) appear mainly during periods without inversion or with a slight inversion (local advection inversion). Concentrations exceeding the standard observed in the absence of inversion are probably the result of long-distance transport or increased residential heating.

Preprints.org (www.preprints.org) | NOT PEER-REVIEWED | Posted: 6 February 2024 doi:10.20944/preprints202402.0319.v1

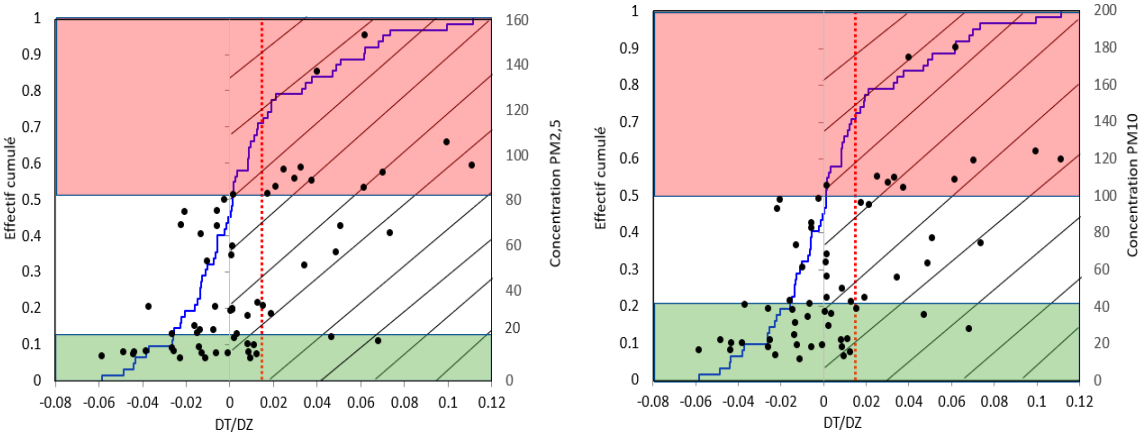

Figure 12. Cumulative distribution of the global ratio ΔT/ΔZ represented in blue and daily average concentrations (µg/m³) as black dots. The red dashed line represents the winter average (γ_{winter}).

3.8. Thermal stratification during persistent pollution episodes

According to WHO guidelines, a day is considered polluted when daily average concentrations exceed the established standards, which are 45 µg/m3 for PM10 and 15 µg/m³ for PM2.5. PM10 levels have exceeded the standard on multiple occasions and over several distinct days. As for the PM2.5 pollutant, it consistently surpassed the standards throughout the winter of 2022/2023 (Figure 13). For the study period, we define a strong pollution episode when concentrations of both pollutants exceed 45 µg/m3 for more than 48 consecutive hours. This value and duration are not defined by specific legislation or agreements regarding air quality. The number 45 is arbitrarily chosen to select pollution days for both pollutants. The 48-hour criterion is established to exclude isolated cases. Moreover, only episodes observed in at least two different locations are considered to identify pollution that is not specifically linked to a single site. The application of these three criteria allows us to detect three distinct episodes during the first two months of the winter of 2022/2023, and their characteristics are listed in Table 3.

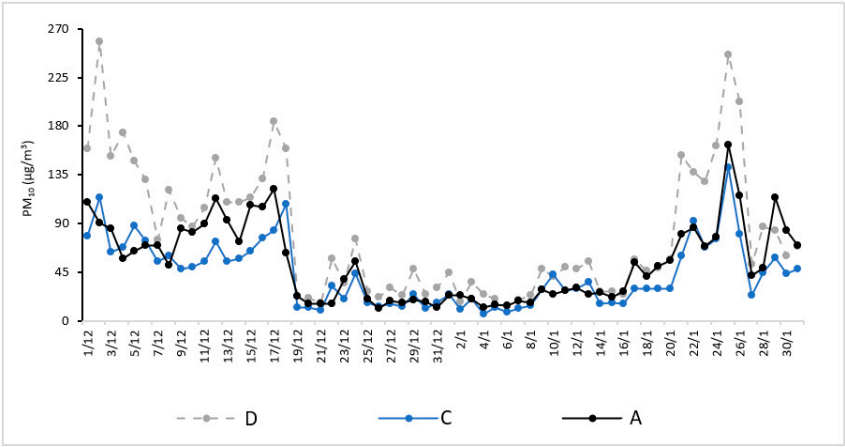

Preprints.org (www.preprints.org) | NOT PEER-REVIEWED | Posted: 6 February 2024 doi:10.20944/preprints202402.0319.v1

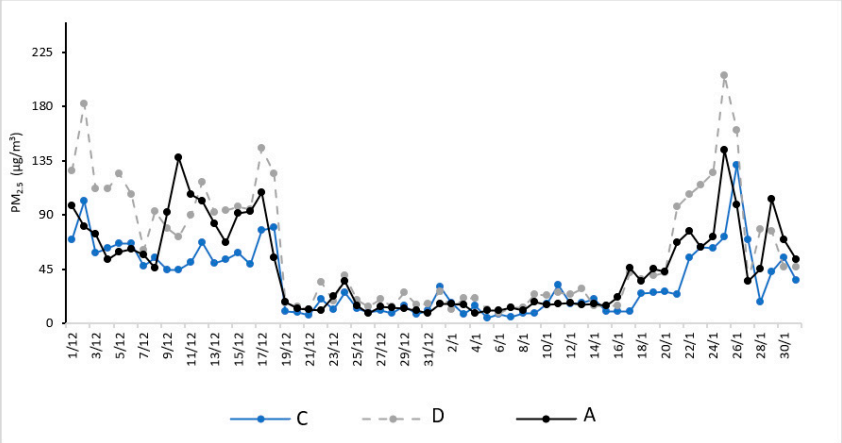

Figure 13. Variation in daily average concentrations of PM10 and PM2.5.

Table 3. Characteristics of the three identified pollution episodes based on the criteria mentioned in the text.

		Episode 1	Episode 2	Episode 3		Episode 1	Episode 2	Episode 3
Average (µg/m³)		104.61	90.50	65.71		77.01	101.58	51.30
Max (µg/m³)	PM_{10}	265.00	256.94	116.95	$PM_{2.5}$	181.95	244.93	103.08
Min (µg/m³)		48.26	29.42	18.81		44.06	14.10	13.21
Persistence		01/12- 18/12	*17/01- 25/01*	27/01- 31/01		01/12- 18/12	*21/01-25/01*	27/01- 31/01

Figure 14 depicts the temporal evolution of temperatures recorded by the "Ecosmart" ground stations and climatic parameters from the conventional meteorological station. It is noteworthy that temperatures follow a distinct pattern compared to pollutants, as evidenced by a correlation coefficient of -0.91. Temperatures are generally low during days marked by pollution episodes, often below 7°C, reaching a minimum of -3°C. When near-surface air masses are cold, they inhibit upward movements, leading to pollutant accumulation. Additionally, pollutant concentrations are influenced by increased residential heating during cold days. Several days of thermal inversions are observed in association with calm winds and clear skies.

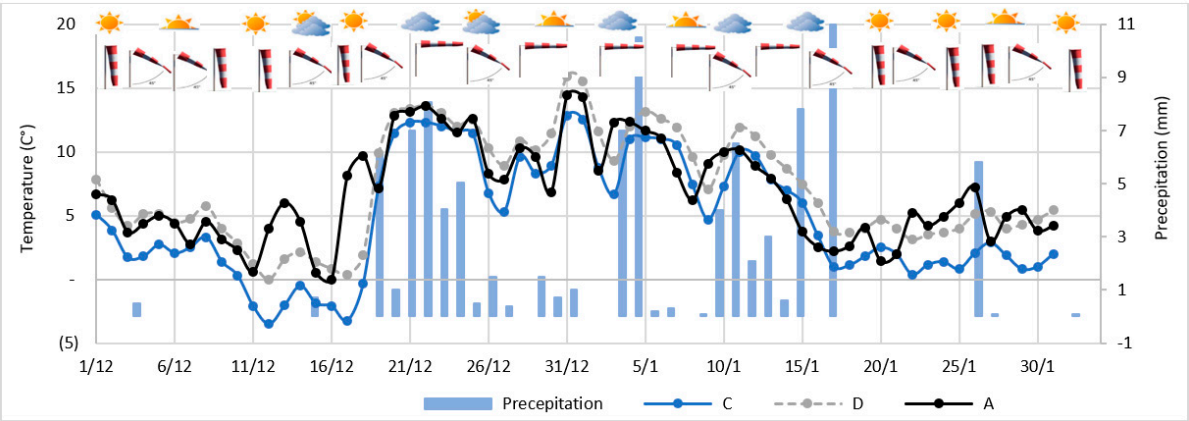

Figure 14. Temporal evolution of hourly temperatures recorded at 00h from the "Ecosmart" ground-based stations.

The first pollution episode (Episode 1) corresponds to localized, low-intensity inversions at the beginning and a persistently strong inversion towards the end. The other two episodes (Episodes 2 and 3) are characterized by persistently stable inversion situations. These three episodes also

 doi:10.20944/preprints202402.0319.v1

coincide with inversions recorded by Trappes. Conversely, days outside of these episodes do not replicate the observed stratification trend. Temperatures exhibit higher values, ranging between 14 and 5°C. On these days, turbulent mixing homogenizes temperatures compared to pollution episode situations where atmospheric stability results in temperature variations. The low particle concentrations are explained by the dispersion and wet deposition of pollution in the presence of an unstable boundary layer associated with high temperatures and significant precipitation.

4. Discussion and conclusion

This study was conducted to characterize the effect of meteorological conditions on particulate concentrations in the Cergy-Pontoise urban area. The annual and monthly variability of PM10 pollution days and their correlation with the vertical temperature profile was assessed at the reference station in Trappes, located 30 km from the study area. We demonstrated that regional-scale temperature inversions were observed to have a significant impact on particle evolution. The results revealed that pollution occurs more frequently during the winter period and persistent inversions with the onset of daylight. This conclusion is consistent with the work of Niedźwiedź et al. (2021) [13], conducted in southern Poland, which shows that the maximum concentration of PM10 occurs during persistent inversion episodes.

While Trappes' radiosondes can trace the thermal structure of the atmospheric layer at the regional scale for pollution days and accurately capture its temporal dynamics, monitoring the urban layer for the agglomeration using a conventional station located 30 km away is incompatible with the space and timescale considered. We then studied the topographic effects on thermal inversions and air quality using locally collected temperature and particle data. We used altitude differences between multiple ground temperature sensors and captive balloon radiosondes to construct a temperature gradient indicative of inversion strength in the Oise Valley.

The methodology developed during this study constituted a successful test to obtain a fine-scale representation of atmospheric dynamics. The system allowed the identification, in addition to regional-scale inversions, of advection-type inversions between the plateau and the bottom of the Oise Valley. The inversions obtained through local measurements in the Oise Valley at the heart of the agglomeration are considered more accurate and sensitive to more local altitude variations (19-200 m). However, a temperature disparity between ground measurements and balloon-sonde measurements is evident, especially at altitudes exceeding 25 meters. Temperatures measured by balloon-sonde indicate higher values compared to ground sensor readings on the western slope. This disparity is explained by the radiative constraints suffered by the atmosphere near the surface, where the sensors are located, unlike measurements made in the valley's atmosphere. The air above the ground cools, leading to the creation of a downslope wind along the slope, carrying a mass of cold air over the slopes. Consequently, the temperature is lower on the slope than in the free atmosphere of the valley at the same altitude [35,36]. On the eastern slope, temperatures are slightly higher due to the warming of the air adjacent to the surface, induced by the sensible heat flux from urban substrates combined with the evacuation of fresh air towards the bottom of the basin.

The analysis of both PM fractions to the locally calculated temperature gradient revealed the existence of a relatively strong correlation between ground inversion and PM. It is shown that concentrations increase as the inversion develops. These results are consistent with Allard's study (2019) [27] in the Arve Valley, emphasizing a strong relationship between winter particulate concentrations and the temperature gradient (ΔT), especially when it reaches high values. Whiteman et al. (2014) [37] also highlight the close link between PM2.5 concentrations and atmospheric stability in deep valleys in winter, suggesting that strong winter pollution must be linked to inversions over several days.

Sometimes high concentrations are observed when the local-scale thermal gradient becomes negative, suggesting that pollution is not necessarily the result of an inversion but also long-distance transport and residential heating, in line with studies by Pateraki et al. (2012) [7,38] distinguishing pollution episodes related to temperature inversions from those induced by long-distance transport.

In the future, we plan to deepen our understanding of thermal inversions by exploring the role of synoptic conditions, such as high and low-pressure systems, atmospheric fronts, and other meteorological elements. By integrating these synoptic factors into our analysis, we hope to obtain a more comprehensive and accurate understanding of the mechanisms responsible for the formation, maintenance, and dissipation of thermal inversions. This comprehensive approach could help anticipate meteorological conditions favorable to the formation of thermal inversions, crucial for the management and prevention of atmospheric pollution episodes.

Author Contributions: Conceptualization, Souad Lagmiri, and Salem Dahech.; Methodology, Souad Lagmiri.; Software, Souad Lagmiri.; Validation, Salem Dahech.; Formal Analysis, Souad Lagmiri.; Investigation, Souad Lagmiri.; Resources, Souad Lagmiri and Salem Dahech.; Data Curation, Souad Lagmiri.; Writing—Original Draft Preparation, Souad Lagmiri.; Writing—Review & Editing, Souad Lagmiri and Salem Dahech.; Visualization, Salem Dahech and Souad Lagmiri.; Supervision, Salem Dahech.; Project Administration, Souad Lagmiri and Salem Dahech.; Funding Acquisition, Souad Lagmiri and Salem Dahech.

Funding: This research was funded by the DIM Qi 2 program of the Île-de-France region and the Cergy-Pontoise agglomeration.

Institutional Review Board Statement: Not applicable.

Informed Consent Statement: Not applicable.

Data Availability Statement: The raw data supporting the conclusions of this article will be made available by the authors on request.

Conflicts of Interest: The authors declare no conflict of interest. The sponsors had no role in the design, execution, interpretation, or writing of the study.

References

1. **Hufty** A. (1976). Introduction à la climatologie. Paris, P.U.F., collection Magellan, 264p.
2. **Li** Z., Guo J., Ding A., Liao H., Liu J., Sun Y., ... Zhu B. (2017a). Aerosol and boundary layer interactions and impact on air quality. Natl. Sci. Rev. 4 (6), 810–833. https:// doi.org/10.1093/nsr/nwx117.
3. **Joly** D and Richard Y. (2022). Temperature inversions in France – Part B: Spatial variations. *Climatol*, **19,5** : 17 p. https://doi.org/10.1051/climat/20221900.
4. **Kassomenos** P.A and Koletsis I.G.: (2005). Seasonal variation of the temperature inversions over Athens, Greece. Int. J. 2005. Climatol. 25: 1651–1663. DOI: 10.1002/joc.1188.
5. **Bourne** S.M., Bhatt U.S., Zhang J., Thoman R. (2010). Surface-based temperature inversions in Alaska from a climate perspective. Atmospheric Research 95 (2010) 353–366. doi:10.1016/j.atmosres.2009.09.013.
6. **Chen** Tianmeng., Guo Jianping., Tong Bing., Cohen Jason Blake., Chen Xinyan., Yun Yuxing., Lv Min., Guo Xiaoran., Lee Seoung Soo. (2022). Elucidating the impact of high- and low-pressure systems on temperature inversion from nine years of radiosonde observations in Beijing. Atmospheric Research 271 (2022) 106115. https://doi.org/10.1016/j.atmosres.2022.106115.
7. **Largeron** Yann and Chantal Staquet. (2016). Persistent inversion dynamics and wintertime PM10 air pollution in Alpine valleys. Atmospheric Environment. Volume 135, June 2016, Pages 92-108. https://doi.org/10.1016/j.atmosenv.2016.03.045.
8. **Gramsch** E., Caceres D., Oyola P., Reyes F., Vasquez, Y., Rubio, M.A., Sanchez G. (2014). Influence of surface and subsidence thermal inversion on PM2.5 and black carbon concentration. *Atmospheric Environment*, *vol. 98.* Pages 290-298. https://doi.org/10.1016/j.atmosenv.2014.08.066.
9. **Lyman** Seth and Tran Trang. (2015). Inversion structure and winter ozone distribution in the Uintah Basin, Utah, U.S.A. Atmospheric Environment 123 (2015) 156-165. http://dx.doi.org/10.1016/j.atmosenv.2015.10.067.
10. **Xu** Tingting., Song Yu., Liu Mingxu., Cai Xuhui., Zhang Hongsheng., Guo Jianping., Zhu Tong. (2019): Temperature inversions in severe polluted days derived from radiosonde data in North China from 2011 to 2016. Science of the Total Environment 647 (2019) 1011–1020.
11. **El Melki** Taoufik. (2007). Temperature inversions and atmospheric pollution concentrations in the low troposphere of Tunis. Climatologie, vol. 4 (2007) 105-129. doi.org/10.4267/climatologie.773.
12. **Kukkonen** J., Pohjola M., et al. (2005). Analysis and evaluation of selected local-scale PM10 air pollution episodes in four European cities: Helsinki, London, Milan, and Oslo. Atmos. Environ., 39 (15) (2005), pp. 2759-2773.
13. **Niedźwiedź** Tadeusz., Łupikasza Ewa Bożena., Małarzewski Łukasz., Budzik Tomasz. (2021). Surface-based nocturnal air temperature inversions in southern Poland and their influence on PM10 and

PM2.5 concentrations in Upper Silesia (2021). Theoretical and Applied Climatology https://doi.org/10.1007/s00704-021-03752-4.

14. **Brulfert** Guillaume. (2004). Modélisation des circulations atmosphériques pour l'étude de la pollution des vallées alpines. Physique [physics]. Université Joseph-Fourier - Grenoble I, 2004. Français. ⟨NNT : ⟩. ⟨tel-00007982⟩.
15. **Allard** Julie. (2018). Qualité de l'air dans la Vallée de l'Arve : météorologie locale et mesures des réductions des émissions liées au chauffage au bois. Ingénierie de l'environnement. Université Grenoble Alpes, 2018. Français. ffNNT : 2018GREAU020ff. fftel-01901636f.
16. **Martin** N. (2008). La pollution par l'ozone et la climatologie dans un espace méditerranéen : les Alpes Maritimes. Géographie. Thèse de doctorat, Université Nice Sophia Antipolis, 2008. Français. NNT: tel-00358297f.
17. **Diaf** N., Bouchaour M., Merad L. et Benyoucef B. (2003). Paramètres Influençant la Dispersion des Polluants Gazeux. Rev. Energ. Ren.: ICPWE (2003)139-142.
18. **SCHOENEICH** Philippe. (2012). MICROCLIMAT D'UNE COMBE FROIDE DU JURA (REGION DU MARCHAIRUZ, VAUD, SUISSE). 25ème Colloque de l'Association Internationale de Climatologie, Grenoble 2012.
19. **Michelot** N. (2014). *L'influence des topoclimats sur la pollution de l'air aux particules dans le sud-ouest des Alpes-Maritimes*. Thèse de Doctorat, Université de Nice Sophia-Antipolis, 416 p.
20.
21. **Demangeot** Jean. (1960). Le climat du Gran Sasso d'Italia. In: *Méditerranée*, 1e année, n°4, 1960. pp. 95-132. DOI: https://doi.org/10.3406/medit.1960.997. www.persee.fr/doc/medit_0025-8296_1960_num_1_4_997.
22. **SABATIER** Tiphaine. (2018). Circulations à fine échelle et qualité de l'air hivernal dans une vallée alpine urbanisée. Thèse de de doctorat à l'Université Toulouse 3 - Paul Sabatier.
23. **Hertig** J.-A. (1995). ASPECTS DE CLIMATOLOGIE DES VILLES SUISSES. CAS DE BIENNE ET DES VILLES DU BASSIN LEMANIQUE. Journée du CUEPE 1995 "Energie et climat urbain", Genève le 1er décembre 1995.
24. **Whiteman**, C. D., Hubbe J. M., and Shaw W. J. (2000). Evaluation of an inexpensive temperature data logger for meteorological applications. J. Atmos. Oceanic Technol., 17, 77–81. DOI: https://doi.org/10.1175/1520-0426(2000)017<0077:EOAITD>2.0.CO;2.
25. **Cordeiro** António M., Rochette Alexandre Ornelas and Djime Dourado Silva. (2023). The Importance of Topography in the Formation of Cold-Air Pooling in Urban Spaces. The Example of the City of Coimbra (Portugal). Theoretical and Applied Climatology 152.1-2 227–239.
26. **Silcox** GD., Kelly KE., Crosman ET., Whiteman CD et Allen BL. (2012). Concentrations hivernales de PM 2,5 lors de mares d'air froid persistantes sur plusieurs jours dans une vallée de montagne. Atmos. Environ. 46, 17–24.
27. **Allard** Julie., Chevrier Florie., Laurent Jean-Paul., Coulaud Catherine., Paci Alexandre., Jezek Irena., Mocnik Grisa., Brulfert Guillaume., Besombes Jean-Luc., Jaffrezo Jean-Luc. (2019). Un système de mesure de température pour suivre l'influence de la stabilité atmosphérique sur la qualité de l'air dans la vallée de l'Arve. La Météorologie - n° 106.
28. **Carrega** Pierre. (2013). The urban climate of Nice (France) in a context of contrasted topography: synthesis using an inductive approach. Climatologie, vol. 10 : 9-34. https://doi.org/10.4267/climatologie.75.
29. **Joly** D and Richard Y. (2019). Frequency, intensity, and duration of thermal inversions in the Jura Mountains of France. Theoretical and Applied Climatology, 138(1), 639–655. https://doi.org/10.1007/s00704-019-02855-3.
30. **Enzo** Le Bouëdec. (2021). Wintertime characteristic atmospheric circulation in the Grenoble basin and impact on air pollution. Meteorology. Université Grenoble Alpes [2020-..], 2021. English. ⟨NNT : 2021GRALU031⟩. ⟨tel-04148049⟩.
31. **Fallot** J.(1991). Etude de la ventilation de la vallée de la Sarine en Gruyère, Geogr. Helv., 46, 32–41, https://doi.org/10.5194/gh-46-32-1991, 1991.
32. **Zhong** S., Shaw W. J., Hubbe J. M., Bian X., and Mittelstadt J. (2001). Cold pools in the Columbia basin. Wea. Forecasting, 16, 432–447.
33. **Wu** Wanning., Zha Yong., Zhang Jiahua., Gao Jay., He Junliang. (2014). A temperature inversion-induced air pollution process as analyzed from Mie LiDAR data. Science of the Total Environment 479–480 (2014) 102–108. http://dx.doi.org/10.1016/j.scitotenv.2014.01.112.
34. **CDVO :** Conseil départemental du val d'Oise. (2019). Données de circulation de 2019. pages 20-42.
35. **Whiteman** C.D., Eisenbach S., Pospichal B., Steinacker R. (2004). Comparison of vertical soundings and sidewall air temperature measurements in a small Alpine basin. J. Appl. Meteorol., 43, 1635-1647.
36. **Whiteman** CD. (2000). Mountain Meteorology: Fundamentals and Applications. Oxford University Press, 355 pp.
37.

 doi:10.20944/preprints202402.0319.v1

38. **Pateraki** S. , Asimakopoulos D. , Flocas H. , Maggos T. , Vasilakos C. (2012). The role of meteorology on different-sized aerosol fractions (PM10, PM2.5, PM2.5-10). Sci. Total Environ., 419 (0) (2012), pp. 5124-5135.